ADVANCED FUNCTIONAL MATERIALS
www.afm-journal.de

Hierarchical Tubular Structures Composed of Mn-Based Mixed Metal Oxide Nanoflakes with Enhanced Electrochemical Properties

Yan Guo, Le Yu, Cheng-Yang Wang, Zhan Lin, and Xiong Wen (David) Lou**

In this work, a simple strategy is developed to synthesize hierarchical tubular structures (HTS) of Mn-based (Co-Mn, Ni-Mn, Cu-Mn, Zn-Mn) mixed metal oxides. The first step in the synthesis involves redox reaction mediated growth of nanoflakes on carbon nanofibers under hydrothermal conditions. After calcination in air, carbon nanofibers are removed and HTS of mixed metal oxides can be obtained with little structural deterioration. The resultant HTS are advantageous as electrodes for electrochemical energy storage. As an example, it is shown that the Co-Mn-HTS sample exhibits outstanding electrochemical performance as electrode materials for hybrid supercapacitors and lithium ion batteries.

1. Introduction

With the foreseeable exhaustion of fossil resources and the increasing negative environmental impact, there is intense worldwide activity to develop more sustainable and renewable energy resources.[1] Consequently, the development of high-efficiency energy storage technologies is indispensable to store the electric energy generated and to stabilize the electricity grid connected.[1,2] In this regard, hybrid supercapacitors (HSCs) and lithium ion batteries (LIBs) are two major types of electrochemical energy storage devices, both of which store electricity in electrochemical processes.[3–5] Numerous efforts have been devoted to develop novel and high-performance electrode materials with the aim to realize high-efficiency energy storage with higher energy/power density, longer cycle life, and lower cost.[3,4,6–8]

Y. Guo, L. Yu, Prof. X. W. Lou
School of Chemical and Biomedical Engineering
Nanyang Technological University
62 Nanyang Drive, Singapore 637459, Singapore
E-mail: xwlou@ntu.edu.sg
Y. Guo, Prof. C.-Y. Wang
Key Laboratory for Green Chemical Technology
of Ministry of Education
School of Chemical Engineering and Technology
Tianjin University
Tianjin 300072, P. R. China
Prof. Z. Lin
Institute of Chemical Engineering
College of Chemical and Biological Engineering
Zhejiang University
Hangzhou, Zhejiang 310027, P. R. China
E-mail: zhanlin@zju.edu.cn

DOI: 10.1002/adfm.201501974

Among all available materials, Mn-based oxides have attracted considerable attention due to their environmentally benign nature and rich redox reactions involving different ions.[9,10] However, the employment of Mn-based oxides is still largely hampered by their intrinsic low charge/ionic conductivity and pronounced volume expansion and contraction during charging/discharging processes, resulting in the pulverization of electrode film.[11–13] In recent years, mixed metal oxides (MMOs), especially single-phase ternary metal oxides with two different metal cations, are emerging as promising electrode materials for energy conversion and storage.[4,5] Benefiting from complex chemical composition and enhanced electrical conductivity, these MMOs are able to effectively enhance the electrochemical performance compared to corresponding monometal oxides.[14–16] In view of the above-mentioned considerable advantages, manganites of transition and/or post transition metals, that is, M-Mn (M = Co, Ni, Zn, etc.) oxides are suggested to be appealing alternatives for high-performance electrochemical energy storage devices.[17–24]

Besides the desirable composition, the electrochemical performance of energy storage devices also highly depends on the microstructure/texture of the electrode materials.[9,25] An emerging and effective avenue is the rational design and synthesis of active materials with hierarchical tubular structures (HTS). These one-dimensional (1D) HTS usually constructed by two-dimensional subunits can effectively alleviate the volume variation, offer an express transport path for electrons and ions and maximize the active interfacial sites,[26,27] thereby providing unusual advantages over the traditional bulk materials as ideal electrode structures.[28,29] To date, it has been widely demonstrated that complex micro-/nanostructures of MMOs with 1D tubular feature could enhance their electrochemical performance.[30–32] For example, Chen and co-workers reported the synthesis of 1D MMOs with complex architectures through controllable single-spinneret electrospinning technique. Especially, the $NiCo_2O_4$ tube-in-tube structures demonstrate superior electrochemical performance in HSCs.[30] Also, our group has recently developed a general strategy to fabricate complex tube-in-tube hollow structures for various MMOs using carbon nanofibers as the hard template. The as-obtained $ZnCo_2O_4$ HTS present good lithium storage properties with remarkable capacity retention.[33] Despite these achievements mentioned above, simple and general synthesis of MMO HTS

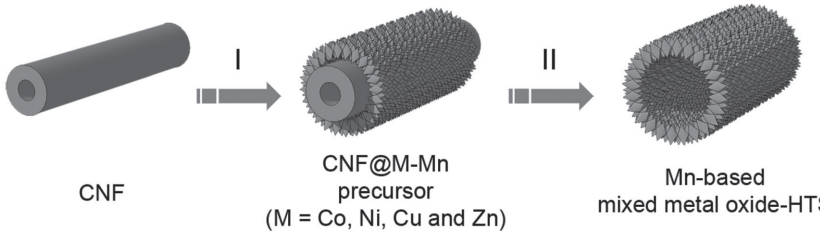

Figure 1. Schematic illustration of the formation of HTS of Mn-based mixed metal oxides. Stage I: formation of CNF@M-Mn core-shell precursor through a facile hydrothermal method. Stage II: formation of Mn-based mixed metal oxide-HTS through a simple annealing treatment in air.

is still considered a challenging task for large scale applications. The progress is usually limited by the requirement of special instruments and lack of template that can be synthesized in large scale.[34] Therefore, it will be of great significance to develop simple and highly efficient synthesis strategy to fabricate Mn-based MMOs with complex tubular structures and controllable composition at a relatively low cost.

Herein, we present a general and cost-effective method for synthesis of Mn-based MMO HTS constructed by ultrathin nanoflakes. The formation is accomplished by redox reaction between $KMnO_4$ and commercially available carbon nanofibers (CNFs) in the aqueous solution in presence of M^{2+} (M = Co, Ni, Cu, and Zn) followed by controlled calcination. As a typical example, the as-synthesized Co-Mn-HTS material has been evaluated as electrode materials for both HSCs and LIBs, and shown to exhibit excellent electrochemical performance with high capacitance/capacity and good cycling stability.

2. Results and Discussion

Novel HTS of Mn-based MMOs are obtained via a facile hydrothermal and subsequent annealing method, as illustrated by the scheme in **Figure 1**. In stage I, core-shelled CNF@M-Mn-precursor nanocables are synthesized by a facile hydrothermal method in presence of M^{2+} cations (M = Co, Ni, Cu, and Zn). Due to the strong redox reaction between $KMnO_4$ and CNFs, the as-formed M-Mn precursor with ultrathin flake-like subunits is grown readily around the CNF surface to form the 1D CNF@M-Mn precursor core-shell structure. During the reaction, the M^{2+} ions can be simultaneously incorporated into the M-Mn precursors. In stage II, the CNFs template is removed through thermal treatment in air to generate HTS of MMOs.

We first carry out morphological analysis on the CNF@Co-Mn-precursor and derived Co-Mn-HTS to study the typical synthesis procedure. The commercial CNFs are in fact carbon nanotubes in nature with a diameter about 100–200 nm and a length over tens of micrometers (Figure S1, Supporting Information). The low-magnification field-emission scanning electron microscopy (FESEM) image reveals that the Co-Mn-precursor shell is uniformly grown along the longitudinal axis of CNFs leading to an increased diameter around 400–500 nm (Figure S2a, Supporting Information). The magnified FESEM images (**Figure 2**a,b) demonstrate that the CNF@Co-Mn-precursor shell is constructed by randomly oriented ultrathin nanoflakes, which are interconnected with each other to form a hierarchical framework. The formation of core-shell structures is further evidenced by transmission electron microscopy (TEM, Figure 2c) observation, as characterized by radial assembly of numerous nanoflakes on the curvature of CNF backbones. It should be mentioned that all the reactants ($KMnO_4$, CNFs, and cobalt source) play vital roles in the control of the morphology and composition for the reaction product (Figure S3, Supporting Information). Without adding cobalt source, $KMnO_4$ can react with CNFs to form inhomogeneous MnO_2 nanoflakes around fibers. Meanwhile, Co-Mn-based hierarchical spheres with smaller flakes are generated in the absence of CNFs. Moreover, no reaction takes place between the cobalt salt and CNFs. The energy-dispersive X-ray (EDX) elemental mapping images based on an individual CNF@Co-Mn-precursor core-shell structure confirm the coexistence and uniform distribution of Co, Mn and O elements within the Co-Mn shell (Figure S4, Supporting Information). The broad and poorly defined peaks shown on the X-ray diffraction (XRD) pattern (Figure S5, Supporting Information) might be assigned to K-birnessite type layer-structured MnO_2 phase (JCPDS Card No. 80–1098). The absence of any diffraction peak originating from cobalt-containing species may be due to the complete incorporation of Co into lattice of manganese oxide.[35,36] Thermogravimetric analysis (TGA) of the core-shell CNF@Co-Mn-precursor (Figure S6, Supporting Information) indicates the weight loss is mainly due to the dehydration/dihydroxylation process and combustion of CNFs.

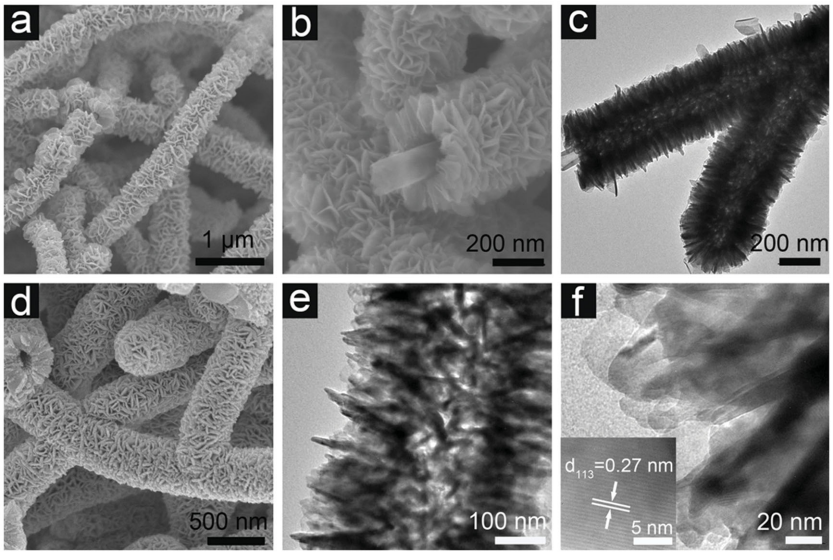

Figure 2. FESEM and TEM characterizations of a–c) CNF@Co-Mn-precursor and d–f) Co-Mn-HTS. The inset of (f) shows a HRTEM image of Co-Mn oxide nanoflakes.

On the basis of the TGA result, a temperature of 500 °C is chosen as the calcination temperature. After annealing in air, the CNF@Co-Mn-precursor is converted to poorly crystallized Co-Mn mixed oxide (the sample is designated as Co-Mn-HTS) and the crystal phase from the XRD pattern (Figure S7a, Supporting Information) might be similar to tetragonal (Co, Mn)(Co, Mn)$_2$O$_4$ phase (JCPDS Card No. 18–0408). No additional signals from possible residues or contaminants can be detected. The sample is further examined by EDX (Figure S8, Supporting Information), which proves the coexistence of Co and Mn elements in the HTS with a Mn/Co atomic ratio of around 1.79, which is much higher than the atomic ratio of Mn/Co in the initial reaction solution. As presented in Figure 2d, the overall 1D morphology of precursor is perfectly retained after calcination. In agreement with FESEM observations, the well-defined inner cavity of the hollow architecture is clearly elucidated by the sharp contrast between the center and the edge (Figure 2e). From the enlarged TEM image in Figure 2f, it can be clearly observed that the complex hierarchical shell structure is constructed by flake-like subunits with a thickness of several nanometers. In virtue of the unique structural features, the Co-Mn-HTS sample manifests a high Brunauer–Emmett–Teller (BET) specific surface area of 60.8 m^2 g^{-1} (Figure S9, Supporting Information). A representative high-resolution TEM (HRTEM) image (inset in Figure 2f) displays the distinct lattice fringes with an interlayer spacing of 0.27 nm, which might be indexed to (113) planes of tetragonal (Co, Mn)(Co, Mn)$_2$O$_4$ crystals. The selected-area electron diffraction (SAED) pattern (Figure S10, Supporting Information) further confirms the polycrystalline feature and all the diffraction rings can be readily indexed to the (Co, Mn)(Co, Mn)$_2$O$_4$ phase.

Importantly, this present approach can be easily extended to prepare HTS of other Mn-based MMOs. For example, we have successfully synthesized various CNF@M-Mn (M = Ni, Cu, and Zn) precursors by replacing of $CoSO_4$ with $NiSO_4$, $CuCl_2$, and $ZnSO_4$ as the reactants (Figure S2, Supporting Information). FESEM results (**Figure 3**a–c) reveal that similar HTS composed of ultrathin nanoflakes are obtained after CNFs are completely combusted in air. However, their plate-like subunits become smaller in size with loose connections. EDX spectra (Figure 3d–f) of the samples derived from CNF@M-Mn precursors (M = Ni, Cu, and Zn) confirm the coexistence of Mn/Ni, Mn/Cu, and Mn/Zn elements in the HTS with atomic ratio of 2.02, 1.63, and 2.19, respectively. Combined with the corresponding XRD analysis (Figure S7, Supporting Information), the crystal phases of these HTS might be assigned to $Ni_{2/3}Mn_{4/3}O_3$, $CuMn_2O_4$, and $ZnMn_2O_4$.

As a demonstration, the as-prepared Co-Mn-HTS sample is first evaluated as an electrode material for HSCs to highlight the merits of these unique architectures. FESEM images of Co-Mn-HTS electrode surface (Figure S11, Supporting Information) show that the robust hollow structures can survive the electrode fabrication process. The cyclic voltammetry (CV) measurments of the Co-Mn-HTS electrode, shown in **Figure 4**a, are performed at various scan rates of 5, 10, 20, and 30 mV s^{-1} in the voltage range of 0 to 0.65 V versus a standard calomel electrode (SCE). Apparently, two typical pairs of redox peaks clearly reveal typical faradaic behaviour of the battery-type electrode, which are mainly originated from faradaic redox reactions related to E–O/E–O–OH (E represents Co and Mn) associated with OH$^-$ anions.[23,37–40] With the increase of scanning rate, the current increases accordingly and the shape of the CV curves is well maintained, implying a good rate capability. Galvanostatic charge-discharge measurements are performed in the voltage range of 0 and 0.6 V (vs SCE). The related chronopotentiometry (CP) curves at various current densities from 2 to 40 A g^{-1} are presented in Figure 4b. Obviously, there are distinct voltage plateaus in the discharge process, further supporting its typical Faradaic nature. The current–density dependence of specific capacitance is plotted in Figure 4c. Notably, the Co-Mn-HTS

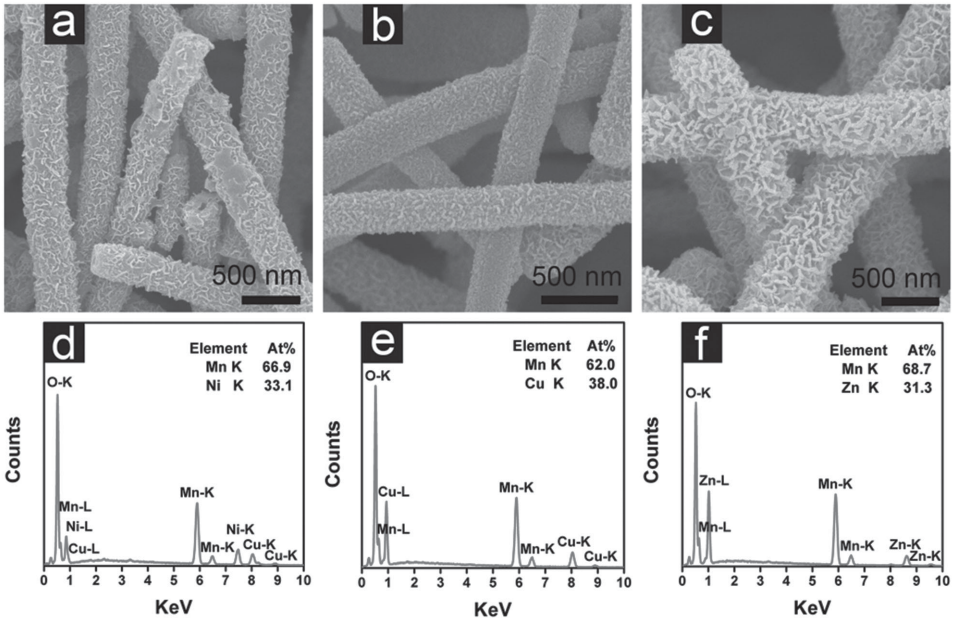

Figure 3. FESEM images a–c) and EDX spectra d–f) of a,d) Ni-Mn-HTS, b,e) Cu-Mn-HTS, and c,f) Zn-Mn-HTS.

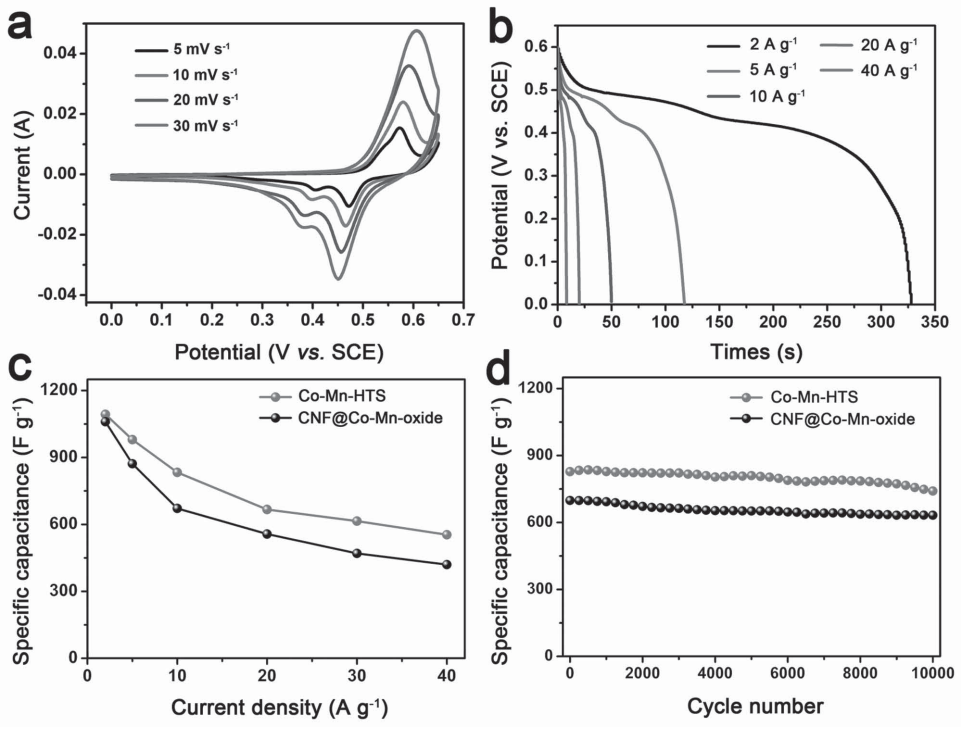

Figure 4. Electrochemical characterizations of the Co-Mn-HTS sample as electrodes for HSCs: a) CV curves at various scan rates, b) discharge voltage profiles at different current densities, c) capacitance as a function of current density, and d) cycling performance at a current density of 10 A g^{-1} for Co-Mn-HTS and CNF@Co-Mn-oxide.

electrode delivers high specific capacitance of 1093, 980, 833, 667, 615, and 554 F g^{-1} at the discharge current densities of 2, 5, 10, 20, 30, and 40 A g^{-1}, respectively. As a reference, the electrochemical performance of the CNF@Co-Mn oxide core-shell composite (Figure S12, Supporting Information) is also provided. From the electrochemical impedance spectroscopy (EIS) measurement, it is clear that the incorporation of CNFs can enhance the electrical conductivity of the CNF@Co-Mn oxide composite compared to the Co-Mn-HTS electrode (Figure S13, Supporting Information). The specific capacitance and rate performance of CNF@Co-Mn oxide are calculated from chronopotentiometry (CP) curves (Figure S14, Supporting Information), which are however much inferior compared to that of Co-Mn-HTS under similar conditions. The lower capacitance of CNF@Co-Mn oxide might be due to the large content of CNFs, which has little contribution to the specific capacitance of the nanocomposite (Figure 14, Supporting Information). The cycling performance of Co-Mn-HTS is studied by repeated charging-discharging tests at a constant current density of 10 A g^{-1}, as shown in Figure 4d. Remarkably, the initial capacitance of Co-Mn-HTS is as high as 809 F g^{-1} with capacitance retention of 91.6% even after 10 000 cycles. Benefiting from the robust support of CNFs, the CNF@Co-Mn oxide electrode shows even better electrochemical stability with higher capacitance retention of 96.9% after 10 000 cycles. Overall, the electrochemical performance of Co-Mn-HTS is comparable to many Co-Mn mixed oxide structures.[14,23,39,41,42] Such desirable electrochemical performance with high capacitance and outstanding cycling stability may be attributed to the unique structure. Specifically, the interconnected ultrathin nanoflakes are in favor of enhancing the contact between electrode material and the electrolyte, which could effectively improve the amount of electroactive sites and electrolyte–electrode interface.[43] Moreover, the empty space in the tubular structure serves as a reservoir for electrolyte which significantly enhances the diffusion kinetics within the electrode.[44]

Furthermore, the Co-Mn-HTS sample is also tested as an electrode material for LIBs to evaluate the electrochemical lithium storage properties. **Figure 5**a shows the galvanostatic discharge-charge voltage profiles of the Co-Mn-HTS electrode for the 1st, 2nd, and 5th cycle in the potential range of 0.05–3 V (vs Li/Li^+) at a current density of 200 mA g^{-1}. The initial discharge and charge capacities can reach as high as 1793 and 1055 mAh g^{-1}, respectively. The initial irreversible capacity loss may be caused by some side reactions such as formation of the solid–electrolyte interface (SEI) layer generated from electrolyte degradation.[45] Nevertheless, the voltage profiles are well overlapping except for the initial discharge, indicating the excellent stability of the structure for reversible lithium storage. The discharge capacity in the range of 1.2–0.4 V is mainly due to reduction from Mn(III) to Mn(II), and the 0.4–0.1 V range reflects the reduction from Mn(II) to Mn(0) and Co(II) to Co(0).[21–23,45] In order to further understand the lithium storage mechanism, CV study is carried out. From the corresponding CV curves (Figure S15, Supporting Information), during the discharge process in the first cycle, two cathodic peaks at ≈1.5 and ≈0.4 V can be identified. These might be attributed to the conversion from Co-Mn mixed oxide to an intermediate-phase MnO and CoO and then to metallic Mn and Co, respectively. There are two indistinct oxidation peaks in the following anodic sweep,

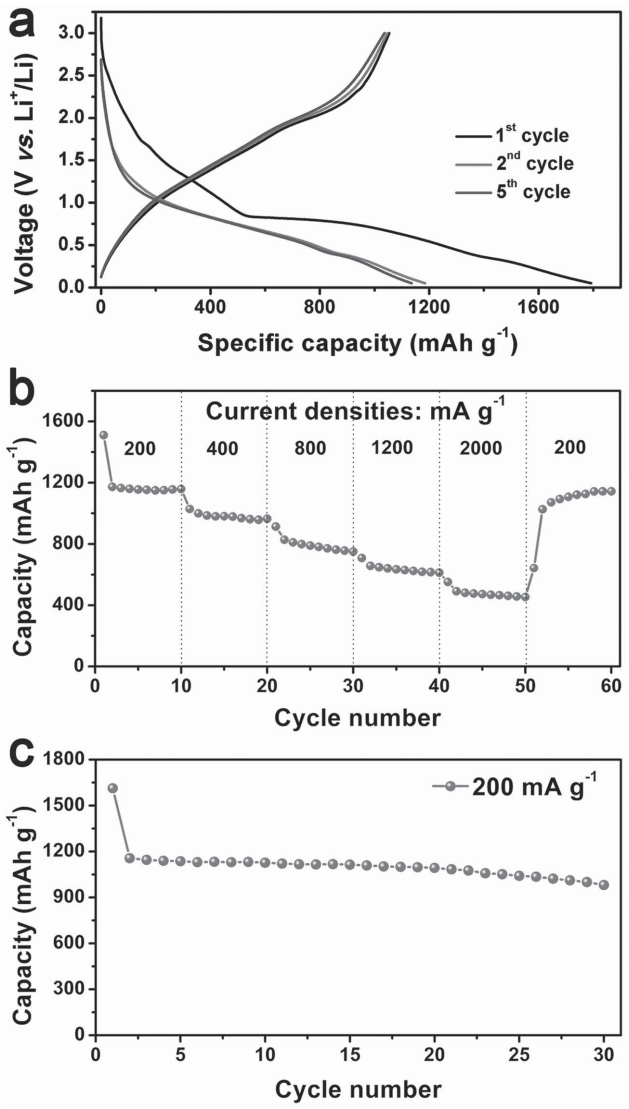

Figure 5. Electrochemical characterizations of the Co-Mn-HTS sample as electrodes for LIBs: a) discharge–charge voltage profiles at a current density of 200 mA g^{-1}, b) rate capability, and c) cycling performance at a current density of 200 mA g^{-1}.

which might correspond to the change of Mn and Co to higher oxidation state(s). From the second cycle onward, the CV profiles are mostly overlapped, indicating good reversibility. As shown in Figure 5b, the Co-Mn-HTS electrode also shows excellent capacity retention at various current densities. The average specific capacities are 1193, 980, 796, 639, and 478 mAh g^{-1} at the current densities of 200, 400, 800, 1200, and 2000 mA g^{-1}, respectively. Moreover, the capacity could recover to almost the original capacity of about 1062 mAh g^{-1} when the current density is reduced to 200 mA g^{-1}. To evaluate the cycling stability, the electrode is charged and discharged at a current density of 200 mA g^{-1}. Despite the relatively large capacity loss in the second cycle, the electrode shows good capacity retention from the second cycle onward and the discharge specific capacity can be maintained at 981 mAh g^{-1} after discharging/charging for 30 cycles (Figure 5c). The outstanding electrochemical performance of Co-Mn-HTS could be attributed to the following factors. First, the nanoflakes shorten the diffusion distance for electrons and Li^+ ions.[46] Second, the cavities in tubular structures could play an important role as ion-buffering reservoirs thus facilitating the rapid Li^+ ions diffusion and at the same time could effectively accommodate the volume change during repeated Li^+ insertion/deinsertion.[21]

3. Conclusions

In conclusion, we have successfully demonstrated a general and cost-effective approach to synthesize hierarchical tubular structures of Mn-based (Co-Mn, Ni-Mn, Cu-Mn, and Zn-Mn) mixed metal oxides constructed by nanoflake subunits via a facile two-step process. As an example, the resultant Co-Mn oxide hierarchical tubular structures manifest excellent electrochemical performance when evaluated as electrode materials for hybrid supercapacitors. Remarkably, the Co-Mn oxide electrode shows excellent cycling stability with capacitance retention of 91.6% after 10 000 charge–discharge cycles. Besides, the Co-Mn oxide sample also exhibits enhanced lithium storage properties. Thus, these hierarchical tubular structures of Mn-based mixed metal oxides may hold great promise for advanced electrochemical energy storage systems.

4. Experimental Section

Pretreatment of Carbon Nanofibers: Carbon nanofibers (CNFs) used in this work were purchased from Sigma-Aldrich Co., Ltd. 0.5 g of the CNFs was refluxed in a mixture of concentrated nitric acid and sulfuric acid (v/v = 3/1) at 100 °C for 4 h. Then, the acid treated CNFs were rinsed with DI water until a neutral pH value was reached. Finally, these samples were collected by filtration and dried for further use.

Synthesis of HTS of Mn-Based Mixed Metal Oxides: The synthesis of HTS of Mn-based mixed metal oxides involves a simple two-step process. Take the synthesis of Co-Mn-HTS as an example. Acid treated CNFs (25 mg) were dispersed in 40 mL of deionized water by sonication, followed by addition of $KMnO_4$ (1 mmol) and $CoSO_4{\cdot}7H_2O$ (1 mmol). The mixture was transferred into Teflon-lined stainless steel autoclave and maintained at 120 °C for 5 h. The precipitate of CNF@Co-Mn-precursor was collected by centrifugation, washed several times with DI water and absolute ethanol, and then dried at 80 °C for 12 h. The CNF@Co-Mn-precursor was converted into Co-Mn-HTS by annealing at 500 °C for 2 h in air, with a ramping rate of 1 °C min^{-1}. As for other Mn-based mixed metal oxide HTS, the synthesis was similar to that of Co-Mn-HTS except that the reactant $CoSO_4{\cdot}7H_2O$ was replaced by $NiSO_4{\cdot}7H_2O$, $CuCl_2{\cdot}2H_2O$ or $ZnSO_4{\cdot}7H_2O$.

Materials Characterization: The microstructure and morphology were investigated using field-emission scanning electron microscope (FESEM; JEOL-6700) and transmission electron microscope (TEM; JEOL, JEM-2010). The composition of the samples was analyzed using energy-dispersive X-ray spectroscope (EDX) attached to the JEOL-6700 microscope. XRD patterns were collected using a Bruker D2 Phaser X-Ray Diffractometer (Cu Kα, λ = 1.5406 Å). Thermogravimetric analysis (TGA) was performed in air with a temperature ramp of 10 °C min^{-1}. The specific surface area and the pore structure of the samples were examined by nitrogen adsorption measurements at 77 K (Autosorb 6B).

Electrochemical Measurements: The working electrode was prepared by mixing the active material, carbon black (super-P-Li), and polymer binder (polyvinylidene difluoride, PVDF) in a weight ratio of 70:20:10. The mixture was then pressed onto the Ni foam and Cu foil as the working electrodes for hybrid supercapacitors and lithium ion batteries,

respectively. Then, the working electrodes were dried at 80 °C for 10 h before test. The loading mass of the active material is about 1 mg cm^{-2}. The electrochemical measurements for hybrid supercapacitor electrode were carried out in an aqueous KOH electrolyte (2.0 M) with a three-electrode cell where a Pt foil served as the counter electrode and a saturated calomel electrode (SCE) was used as the reference. The characterization of the electrode material for LIBs was performed using two-electrode Swagelok-type cells with lithium plate as both the counter electrode and reference electrode. The electrolyte used was 1 M $LiPF_6$ solution in a 1:1 (V:V) mixture of ethylene carbonate and diethyl carbonate. The cell was assembled in an argon-filled glovebox with concentrations of moisture and oxygen below 1.0 ppm. Galvanostatic charging/discharging and cycling tests were performed using a NEWARE battery measurement system. Cyclic voltammetry measurements were conducted on a CHI 660C electrochemical workstation. EIS measurements were carried out by applying an AC voltage with 1 mV amplitude in a frequency range from 0.1 Hz to 100 kHz at open-circuit potential.

Received: May 13, 2015
Revised: June 22, 2015
Published online: July 14, 2015

[1] A. S. Arico, P. Bruce, B. Scrosati, J. Tarascon, W. V. Schalkwijk, *Nat. Mater.* **2005**, *4*, 366.
[2] N. Armaroli, V. Balzani, *Angew. Chem. Int. Ed.* **2007**, *46*, 52.
[3] P. Simon, Y. Gogotsi, *Nat. Mater.* **2008**, *7*, 845.
[4] M. V. Reddy, G. V. Subba Rao, B. V. R. Chowdari, *Chem. Rev.* **2013**, *113*, 5364.
[5] C. Z. Yuan, H. B. Wu, Y. Xie, X. W. Lou, *Angew. Chem. Int. Ed.* **2014**, *53*, 1488.
[6] G. P. Wang, L. Zhang, J. J. Zhang, *Chem. Soc. Rev.* **2012**, *41*, 797.
[7] F. Y. Cheng, J. Liang, Z. L. Tao, J. Chen, *Adv. Mater.* **2011**, *23*, 1695.
[8] P. Poizot, S. Laruelle, S. Grugeon, L. Dupont, J.-M. Tarascon, *Nature* **2000**, *407*, 496.
[9] K. Zhang, X. P. Han, Z. Hu, X. L. Zhang, Z. L. Tao, J. Chen, *Chem. Soc. Rev.* **2015**, *44*, 699.
[10] W. F. Wei, X. W. Cui, W. X. Chen, D. G. Ivey, *Chem. Soc. Rev.* **2011**, *40*, 1697.
[11] X. Lang, A. Hirata, T. Fujita, M. Chen, *Nat. Nanotechnol.* **2011**, *6*, 232.
[12] S. Chen, J. W. Zhu, X. D. Wu, Q. F. Han, X. Wang, *ACS Nano* **2010**, *4*, 2822.
[13] Y. Xia, Z. Xiao, X. Dou, H. Huang, X. H. Lu, R. J. Yan, Y. P. Gan, W. J. Zhu, J. P. Tu, W. K. Zhang, X. Y. Tao, *ACS Nano* **2013**, *7*, 7083.
[14] N. Padmanathan, S. Selladurai, *Ionics* **2014**, *20*, 479.
[15] J. F. Li, S. L. Xiong, Y. R. Liu, Z. C. Ju, Y. T. Qian, *ACS Appl. Mater. Interfaces* **2013**, *5*, 981.
[16] T. Y. Wei, C. H. Chen, H. C. Chien, S. Y. Lu, C. C. Hu, *Adv. Mater.* **2010**, *22*, 347.
[17] F. M. Courtel, H. Duncan, Y. Abu-Lebdeh, I. J. Davidson, *J. Mater. Chem.* **2011**, *21*, 10206.
[18] L. Yu, L. Zhang, H. B. Wu, G. Q. Zhang, X. W. Lou, *Energy Environ. Sci.* **2013**, *6*, 2664.
[19] Y. Y. Yang, Y. Q. Zhao, L. F. Xiao, L. Z. Zhang, *Electrochem. Commun.* **2008**, *10*, 1117.
[20] J. Zhao, F. Q. Wang, P. P. Su, M. G. Li, J. Chen, Q. H. Yang, C. Li, *J. Mater. Chem.* **2012**, *22*, 13328.
[21] J. F. Li, S. L. Xiong, X. W. Li, Y. T. Qian, *Nanoscale* **2013**, *5*, 2045.
[22] L. Zhou, D. Y. Zhao, X. W. Lou, *Adv. Mater.* **2012**, *24*, 745.
[23] Y. N. Xu, X. F. Wang, C. H. An, Y. J. Wang, L. F. Jiao, H. T. Yuan, *J. Mater. Chem. A* **2014**, *2*, 16480.
[24] L. Li, F. He, S. L. Gai, S. H. Zhang, P. Gao, M. L. Zhang, Y. J. Chen, P. P. Yang, *CrystEngComm* **2014**, *16*, 9873.
[25] C. Liu, F. Li, L. P. Ma, H. M. Cheng, *Adv. Mater.* **2010**, *22*, E28.
[26] G. Q. Zhang, X. W. Lou, *Angew. Chem. Int. Ed.* **2014**, *126*, 9187.
[27] C. K. Chan, H. L. Peng, G. Liu, K. McIlwrath, X. F. Zhang, R. A. Huggins, Y. Cui, *Nat. Nanotechnol.* **2008**, *3*, 31.
[28] L. Zhang, G. Q. Zhang, H. B. Wu, L. Yu, X. W. Lou, *Adv. Mater.* **2013**, *25*, 2589.
[29] Q. Li, Z. L. Wang, G. R. Li, R. Guo, L. X. Ding, Y. X. Tong, *Nano Lett.* **2012**, *12*, 3803.
[30] S. J. Peng, L. L. Li, Y. X. Hu, M. Srinivasan, F. Y. Cheng, J. Chen, S. Ramakrishna, *ACS Nano* **2015**, *9*, 1945.
[31] G. Q. Zhang, L. Yu, H. E. Hoster, X. W. Lou, *Nanoscale* **2013**, *5*, 877.
[32] J. G. Kim, S. H. Lee, Y. M. Kim, W. B. Kim, *ACS Appl. Mater. Interfaces* **2013**, *5*, 11321.
[33] G. Q. Zhang, B. Y. Xia, C. Xiao, L. Yu, X. Wang, Y. Xie, X. W. Lou, *Angew. Chem. Int. Ed.* **2013**, *125*, 8805.
[34] K. Wang, Y. Yang, H.-W. Liang, J.-W. Liu, S.-H. Yu, *Mater. Horiz.* **2014**, *1*, 338.
[35] C. L. Tang, X. Wei, Y. M. Jiang, X. Y. Wu, L. N. Han, K. X. Wang, J. S. Chen, *J. Phys. Chem. C* **2015**, *119*, 8465.
[36] G. L. Wang, G. J. Shao, J. P. Du, Y. Zhang, Z. P. Ma, *Mater. Chem. Phys.* **2013**, *138*, 108.
[37] Q. Zhou, X. Wang, Y. Liu, Y. He, Y. Gao, J. Liu, *J. Electrochem. Soc.* **2014**, *161*, A1922.
[38] L. Li, Y. Q. Zhang, F. Shi, Y. J. Zhang, J. H. Zhang, C. D. Gu, X. L. Wang, J. P. Tu, *ACS Appl. Mater. Interfaces* **2014**, *6*, 18040.
[39] L. B. Kong, C. Lu, M. C. Liu, Y. C. Luo, L. Kang, X. H. Li, F. C. Walsh, *Electrochim. Acta* **2014**, *115*, 22.
[40] P. Simon, Y. Gogotsi, B. Dunn, *Science* **2014**, *343*, 1210.
[41] J. Gomez, E. E. Kalu, *J. Power Sources* **2013**, *230*, 218.
[42] L. Li, Y. Q. Zhang, X. Y. Liu, S. J. Shi, X. Y. Zhao, H. Zhang, X. Ge, G. F. Cai, C. D. Gu, X. L. Wang, J. P. Tu, *Electrochim. Acta* **2014**, *116*, 467.
[43] T. Zhu, H. B. Wu, Y. B. Wang, R. Xu, X. W. Lou, *Adv. Energy Mater.* **2012**, *2*, 1497.
[44] L. Yu, L. Zhang, H. B. Wu, X. W. Lou, *Angew. Chem. Int. Ed.* **2014**, *126*, 3785.
[45] H. L. Wang, L. F. Cui, Y. Yang, H. S. Casalongue, J. T. Robinson, Y. Y. Liang, Y. Cui, H. J. Dai, *J. Am. Chem. Soc.* **2010**, *132*, 13978.
[46] C. Wang, Y. Zhou, M. Y. Ge, X. B. Xu, Z. L. Zhang, J. Z. Jiang, *J. Am. Chem. Soc.* **2010**, *132*, 46.